Title

Ligand-Induced Proton Transfer and Low-Barrier Hydrogen Bond Revealed by X-ray Crystallography

Journal

Journal of the American Chemical Society, 137(25)

ISSN

0002-7863

Authors

Nichols, Derek A
Hargis, Jacqueline C
Sanishvili, Ruslan
et al.

Publication Date

2015-07-01

DOI

10.1021/jacs.5b00749

Peer reviewed

Published in final edited form as:

J Am Chem Soc. 2015 July 1; 137(25): 8086–8095. doi:10.1021/jacs.5b00749.

Ligand-induced proton transfer and low-barrier hydrogen bond revealed by X-ray crystallography

Derek A. Nichols[1], **Jacqueline C. Hargis**[2], **Ruslan Sanishvili**[3], **Priyadarshini Jaishankar**[4], **Kyle Defrees**[4], **Emmanuel Smith**[1], **Kenneth K. Wang**[2], **Fabio Prati**[5], **Adam R. Renslo**[4], **H. Lee Woodcock**[2], and **Yu Chen**[1,*]

[1]University of South Florida College of Medicine, Dept of Molecular Medicine, 12901 Bruce B. Downs Blvd, MDC 3522, Tampa, FL 33612

[2]Department of Chemistry, University of South Florida, Tampa, Florida 33620

[3]GMCA@APS, X-ray Science Division, Advanced Photon Source, Argonne National Laboratory, Argonne, Illinois 60439

[4]Department of Pharmaceutical Chemistry and Small Molecule Discovery Center, University of California San Francisco, 1700 4th Street, Byers Hall S504, San Francisco, CA 94158

[5]Department of Life Sciences, University of Modena and Reggio Emilia, Italy

Abstract

Ligand binding can change the pKa of protein residues and influence enzyme catalysis. Herein, we report three ultrahigh resolution X-ray crystal structures of CTX-M β-lactamase, directly visualizing protonation state changes along the enzymatic pathway: apo protein at 0.79 Å, pre-covalent complex with non-electrophilic ligand at 0.89 Å, and acylation transition state (TS) analog at 0.84 Å. Binding of the non-covalent ligand induces a proton transfer from the catalytic Ser70 to the negatively charged Glu166, and the formation of a low-barrier hydrogen bond (LBHB) between Ser70 and Lys73, with a length of 2.53 Å and the shared hydrogen equidistant from the heteroatoms. QM/MM reaction path calculations determined the proton transfer barrier to be 1.53 kcal/mol. The LBHB is absent in the other two structures although Glu166 remains neutral in the covalent complex. Our data represents the first X-ray crystallographic example of a hydrogen engaged in an enzymatic LBHB, and demonstrates that desolvation of the active site by ligand binding can provide a protein microenvironment conducive to LBHB formation. It also suggests that LBHBs may contribute to stabilization of the TS in general acid/base catalysis together with other pre-organized features of enzyme active sites. These structures reconcile previous experimental results suggesting alternatively Glu166 or Lys73 as the general base for acylation, and underline the importance of considering residue protonation state change when

*To whom correspondence should be addressed. Phone: (813) 974-7809; Fax: (813) 974-7357; ychen1@health.usf.edu.

The coordinates and the structure factors have been deposited in the Protein Data Bank (PDB), www.rcsb.org, with the following accession codes: 4UA6, 4UA7, 4UA9, 4UAA.

Supporting Information Available

The supporting information contains the following: a supplementary table containing relevant hydrogen bond distances and residue bond lengths, supplementary table with X-ray data collection and refinement statistics, and a supplementary figure which includes an additional ultra high resolution complex structure showing the LBHB between Lys73 and the catalytic Ser70 in the active site. This information is available free of charge via the internet at http://pubs.acs.org.

modeling protein-ligand interactions. Additionally, the observation of another LBHB (2.47 Å) between two conserved residues, Asp233 and Asp246, suggests that LBHBs may potentially play a special structural role in proteins.

Introduction

The protonation states of protein side chains dictate their roles in enzyme catalysis and ligand binding. This information, while vital to the study of enzyme mechanisms and drug discovery, is challenging to obtain experimentally, especially for transient reaction intermediates. In particular, the binding of small molecules often modifies the protein microenvironment and consequently the pKa of catalytic residues. Such effects can potentially promote proton transfer in a pre-covalent Michaelis complex and during general acid/base catalysis. This perturbation may also induce the formation of a low barrier hydrogen bond (LBHB), where two functional groups with similar pKa's equally share a proton, thus contributing to an unusually short (~2.5 Å), strong hydrogen bond (HB) [1]. Both experimental [2–5] and computational studies [6–9] support the notion of LBHBs in enzyme catalysis but X-ray crystallographic structural evidence has so far been elusive, primarily due to the experimental challenge of precisely locating hydrogen atom positions and the transient nature of catalytic LBHBs. Meanwhile, opposing arguments supported by experimental and computational analysis have been put forward to challenge the existence of LBHBs in proteins and the contribution of such short LBHBs to enzyme catalysis[10–14].

CTX-M Class A β-lactamase, a member of the serine hydrolase superfamily, provides a suitable system for such investigation because its crystals can diffract to sub-Angstrom resolution and small molecule inhibitors have been developed to probe relevant reaction intermediates [15,16]. CTX-M, the most common clinically observed extended spectrum β-lactamase, has enhanced activity in hydrolyzing and deactivating third-generation cephalosporins, in addition to other common β-lactam antibiotics such as penicillins [17,18]. The enzymatic mechanism includes acylation and deacylation steps, both involving proton transfer facilitated by general-acid/base catalysis. In formation of the initial acyl-enzyme intermediate, Ser70 is deprotonated during its attack on the β-lactam substrate, with a subsequent proton transfer to the nitrogen atom of the scissile bond. Deacylation of the acyl-enzyme intermediate begins when a general base removes a proton from the catalytic water that serves as a nucleophile to react with the acyl-enzyme, releasing the hydrolyzed β-lactam and regenerating the free enzyme.

One outstanding question of Class A β-lactamase catalysis is the identity of the general base in the acylation step; Lys73 and Glu166 have alternately been proposed to play this role [19–25]. A quantum mechanics/molecular mechanics (QM/MM) approach employed by Mobashery and coworkers using TEM-1 Class A β-lactamase supports a concerted base hypothesis, in which substrate binding induces proton transfer from Ser70 via the catalytic water to anionic Glu166 (Fig. 1) with simultaneous proton transfer from Lys73 to Ser70 [26]. This produces a pre-covalent Michaelis complex in which all three residues (Ser70, Lys73 and Glu166) are neutral. Neutral Lys73 will then deprotonate Ser70 during the nucleophilic attack on the β-lactam ring [26]. Confirmation of this hypothesis could potentially reconcile

seemingly contradicting hypotheses suggesting alternatively Lys73 or Glu166 as the general base for the acylation reaction [19–25]. However, verification remains an experimental challenge due to the necessarily transient nature of the Michaelis complex in the case of electrophilic (reactive) β-lactam substrates.

Results

Protonation state change and LBHB observed by X-ray crystallography

Recently, we described a new class of potent but non-electrophilic inhibitors of CTX-M with activity in live bacteria [15]. We considered that these compounds, which interact with many of the same active site residues as β-lactam substrates, might serve to mimic the pre-covalent complex formed transiently with β-lactam substrates. Using one of these new inhibitors and a previously described covalent boronic-acid based inhibitor, we have now elucidated three sub-Angstrom resolution X-ray crystal structures of CTX-M-14, which together capture the first three stages of the enzymatic pathway: apo protein (0.79 Å), pre-covalent ligand complex (0.89 Å), and covalent transition-state analog for the acylation reaction (0.84 Å). Many hydrogen atoms, including some on the ligand, can be identified using unbiased Fo−Fc difference maps calculated with the hydrogen-omitted model (Fig. 2). Significantly, all hydrogen atoms on the polar residues constituting the catalytic machinery can be discerned unambiguously (Fig. 3A–C). Hydrogen atoms are consistently observed in the same location, in both monomers in the asymmetric unit of the $P2_1$ space group, and among data sets obtained from different crystals having similar resolutions (Supplementary Fig. 1).

In the apo structure, Lys73 is protonated and donates a HB to Ser70, which in turn acts as a HB donor to the catalytic water (wat1, Fig. 3A). This same water also donates a HB to Glu166, which is in the carboxylate form. These observations are in accord with a previously determined 0.88 Å resolution X-ray crystal structure of apo CTX-M-9, as well as a 0.90 Å resolution SHV-2 structure [16,21]. Interestingly, a very different hydrogen-bonding network is observed in the complex with non-electrophilic inhibitor **1** (Fig 3B). A net transfer of a proton from Ser70 to Glu166 via the catalytic water has occurred, resulting in a neutral Glu166. Ser70 appears primed for reaction with substrate, and now accepts HB from the catalytic water, and is involved in a very short HB (at a length of 2.53 Å) with Lys73. This protonation state is essentially the same as that predicted previously by QM/MM for the pre-covalent Michaelis complex, with one unexpected and subtle difference. Notably, the Fo−Fc and 2Fo−Fc maps reveal that the hydrogen atom shared by Lys73 and Ser70 is equidistant (1.3 Å) from the two heteroatoms, Lys73Nζ and Ser70Oγ, meeting a key criteria for a LBHB (Fig. 3B, 4A) [13]. The observation of this hydrogen in the 2Fo−Fc map indicates that it is as highly ordered as the hydrogens which are covalently bound to Ser70Cβ and other carbon atoms in the vicinity (Fig 4A). Its location exactly at the center of the HB between Ser70 and Lys73 is observed in both monomers of the asymmetric unit and also in a second structure solved to similar resolutions (Supplementary Fig. 1).

The ability of 2Fo−Fc map to discern highly ordered hydrogens allowed the identification of a second LBHB between two buried aspartate residues (Asp233 and Asp246). This LBHB, unlike the one in the active site, is present in all three structures, and will be discussed more

fully later (Fig. 4B). Aside from the HBs with the catalytic water and Lys73, Ser70Oγ accepts a third HB from the water molecule in the oxyanion hole (wat4). This HB shortens from 2.85 Å in the apo structure to 2.59 Å in the noncovalent complex. This shortening may reflect an increase in the partial negative charge on Ser70Oγ in the non-covalent complex with **1**. The unusually close HB interaction with wat 4 possibly mimics the approach of nucleophilic Ser70Oγ to the electrophilic carbonyl carbon of a bound β-lactam substrate, which would place the carbonyl group roughly in the position of wat 4. In all, Ser70Oγ functions as acceptor in two HBs in addition to the LBHB with Lys73. None of the hydrogen atoms in these three HBs is within covalent bond distance to Ser70Oγ. Although we cannot exclude the possibility that the hydrogen of a protonated Ser70 is simply not observable in the electron density map, we deem this highly unlikely considering Ser70Oγ is already surrounded by three close HB donors. Moreover, as reported earlier in another ultrahigh resolution structure, hydrogen "visibility" inversely correlates with the temperature factor (B factor) of the heavy atom to which it is bound [27]. The B factor of Ser70 Oγ (7.67 $Å^2$) is similar to that of Lys73 Nζ (7.53 $Å^2$) and wat4 (7.31 $Å^2$) and lower than those of Glu166 Oε1 (8.38 $Å^2$) and wat1 (9.32 $Å^2$), all of which are in the vicinity and whose covalently bound hydrogens are clearly visible in Fo−Fc maps (Fig. 3B).

Boronic acid inhibitors like **2** are often employed to mimic the acylation transition state, since they will react with the catalytic serine to form a tetrahedral boronate adduct.[20] In our structure of covalently bound **2**, Glu166 is neutral while Lys73 is protonated (charged) and moves away from the Ser70-boronate adduct and closer to Ser130 (Fig 2B). Ser130 is well positioned to mediate proton transfer to nitrogen in the tetrahedral intermediate of a β-lactam substrate, which is mimicked by a boronate oxygen in the complex with **2** (Fig. 2B). That Glu166 is indeed protonated in complexes with **1** and **2** is further supported by the Cδ-Oε1 bond length, which is 1.26 Å in the apo structure and 1.31 Å in the structures with **1** and **2** (Supplementary Table 1). They also agree with the 0.85 Å resolution X-ray structure of TEM-1 [20] and the 2.0 Å resolution neutron structure of Toho-1 [28], a CTX-M family member, both in complex with a boronic acid covalent inhibitor. In addition to the previously discussed LBHB in the noncovalent complex with **1**, the HB between Glu166 and the catalytic water also appears to be short in both the complexes with **1** and **2**, at a distance of 2.55 Å. However, the shared hydrogen atom, which is clearly visible in the Fo −Fc maps, is covalently bound to Oε1 of Glu166 in both complexes. Among the close, strong hydrogen bonds in the active site, only the HB between Ser70 and Lys73 exhibits all the characteristics of a LBHB.

Protonation state change and LBHB suggested by QM/MM

The protonation state of Glu166 in complex with **1** agrees with the QM/MM predictions of Mobashery et al [26], highlighting the increasing sophistication and maturity of computational modeling in making meaningful predictions for enzyme catalysis. Although this previous study did not investigate the possibility of a LBHB between Ser70 and Lys73, the results did indicate that this HB can be as short as 2.5 Å. Moreover, the QM/MM calculations predicted that the charged $(Lys73\text{-}NH_3)^+$-$(Ser70\text{-}O)^-$ pair will become neutral $(Lys73\text{-}NH_2)$-(Ser70-OH) upon β-lactam substrate binding, and that the proton on Ser70 will transfer to Lys73 as Ser70 attacks the substrate [26]. We previously performed a QM/MM investigation of CTX-M

with the non-covalent β-lactam substrate cefoxitin [29]. Two protonation state combinations were examined as a function of altering the Lys73 and Glu166 protonation state. Upon examining orbital interactions and active site reorganization, we were able to confirm the hypothesis that Lys73 and Glu166 are neutral in the presence of a substrate, concordant with the experimental observations presented here.

While previous computational results align well with the present work's experimental findings [26], the differences between TEM-1 and CTX-M warrant additional investigations that focus on effects induced by the non-covalent inhibitor, the LBHB, and additional water molecules in the active site. To better corroborate experimental findings related to the microenvironment fluctuation, 11 ns molecular dynamics (MD) simulations were performed on three unique protonation state combinations for the CTX-M active site for the complex with **1**. Three states were created to capture the effects that occur in the non-covalent inhibitor complex: state **I,** Ser70 - negatively charged, Glu166 - neutral, and Lys73 - positively charged; state **II,** Ser70 - neutral, Glu166 - neutral, Lys73 - neutral; and state **III,** Ser70 - neutral, Glu166 - negatively charged, and Lys73 - positively charged. Additionally, an apo state was prepared mimicking protonation state **III**.

For states **I** and **II**, the average distance between Lys73Nζ and Ser70Oγ for the 11 ns simulation is 2.55 Å and 2.53 Å, respectively, while for state **III** the average distance is 2.88 Å in the complex with **1**. These results concur with the experimental findings that Glu166 is neutral in the non-covalent inhibitor complex. Further, this evidence agrees with the formation of the LBHB in the non-covalent complex, while the purposefully incorrect protonation state combination (**III**) shows that the LBHB does not occur arbitrarily. Additionally, the average distance of 2.87 Å between Lys73Nζ and Ser70Oγ in the simulation of the apo state is in good agreement with the apo crystal structure.

To better understand the Ser-Lys LBHB, QM/MM calculations were performed to predict the location of the hydrogen atom between Lys73 and Ser70 in addition to the barrier height of the proton transfer. The initial QM/MM minimized structure confirms that the hydrogen energetically prefers being bonded to Ser70. However, due to the transient nature of LBHBs a closer look at the reaction barrier is warranted, and was performed using the QM/MM replica path (RPATH) plus restraint distance (RESD) method [30–34]. The replica framework allows the system to be partitioned into three regions: the QM region (the non-covalent inhibitor, Glu166, Ser70, Lys73, Ser130, Lys234, Thr235, Gly236, Ser237, wat1, and wat4), the replica region, and the MM region. The QM region is treated quantum mechanically and is where the reaction occurs; the replica region (i.e. everything within 6.5 Å of the QM region) is re-minimized with MM as a function of the reaction's propagation in the QM region. Finally, the third partitioned region is calculated via MM and is treated consistently throughout the reaction. The RESD method is utilized in the replica framework and uses a linear combination of distances to drive the movement of the hydrogen atom between Ser70 and Lys73 in increments of 0.10 Å. The energy is computed at each point of the pathway with a correction applied to replicate high level ab initio barriers for LBHBs[35]. The computed barrier is 1.53 kcal/mol, which is well under the threshold that typically indicates a LBHB (Fig. 5). Further, it has previously been shown that the zero point vibrational energy (ZPVE) for LBHBs is approximately 1–2 kcal/mol[35]. Upon applying the typical

LBHB ZPVE to the present system, the barrier is estimated to be ~0.5 kcal/mol. This is lower than kT (0.593 kcal/mol) suggesting that the barrier is thermal and a continuum of states is possible, corroborating experimental evidence. Additional computational evidence also indicates the importance of the enzyme for the formation of the LBHB. Upon computing the proton transfer pathway using only the QM region (i.e., eliminating the MM protein environment), there is a monotonic energy increase of 7.6 kcal/mol as the hydrogen moves from Ser70 to Lys73, suggesting that one protonation state is now energetically much more favored than the other.

LBHB in activating a nucleophilic serine in general base catalysis

The sub-Angstrom resolution crystal structures provide for the first time the experimental evidence to reconcile several decades' mutagenesis/biochemical data and the seemingly contradicting hypotheses on the identity of the general base for the acylation reaction of Class A β-lactamases. Although Glu166 is involved in a proton transfer upon initial ligand binding, Lys73 appears to be the actual general base activating the nucleophilic Ser70 in the pre-covalent complex. The conformational changes of Lys73 in our three structures seem to track the reaction coordinates, consistent with its proposed role at different stages of the reaction (Fig. 3D). Previous kinetic isotope effect (KIE) studies and QM/MM calculations suggest that the formation of the tetrahedral transition state is the rate-limiting step of the acylation reaction during Class A β-lactamase catalysis[26,36]. More specifically, general base catalysis is required to initiate the formation of this tetrahedral TS, whereas general acid catalysis is involved in the collapse of the TS. We propose that our non-covalent complex with **1** captures a reaction state en route to the tetrahedral TS (rather than the ground-state Michaelis complex), and involving general base catalysis (Fig. 3B). After Glu166 extracts the proton from Ser70 through the catalytic water, Lys73 moves closer to Ser70 and lowers the energy barrier of the TS formation through a LBHB (Fig. 3D). In comparison, our covalent complex with **2** mimics a reaction state preceding collapse of the tetrahedral TS (rather than the real TS), when general acid catalysis takes place (Fig. 3C). The Lys73 side chain swings further away from Glu166 and closer to Ser130 (Fig. 2B, 3D), which donates a proton to the ring nitrogen of the substrate and promotes the collapse of the tetrahedral TS. QM/MM calculations have also suggested that, after transferring a proton to Ser130, Lys73 would move back to and extract the proton from Glu166, activating the latter for the deacylation step [26]. Additionally, other active site features, such as the oxyanion hole formed by the backbone amide groups of Ser70 and Ser237, also make important contributions to the stabilization of the TS during this process.

The experimentally observed LBHB between Ser70 and Lys73 suggests the importance of Lys73 in stabilizing the nucleophilic serine in preparation for its attack on the β-lactam substrate. It has long been hypothesized but also a matter of debate that LBHBs can supply up to 10–20 kcal/mol of free energy for enzymatic reactions, significantly higher than approximately 3–5 kcal/mol for a standard HB [1,4]. A recent study has suggested that LBHBs can play a special role in enzyme catalysis to the extent the semi-solid and weakly-polar character of an enzyme active site can support a LBHB with a reasonable fraction of the strengths found in the gas phase [3]. The existence of such LBHBs in proteins however, has been subject to intense debate, partly due to the lack of direct observation by X-ray

crystallography [37,38]. Our structures not only represent the first observation of a hydrogen engaged in such a LBHB by X-ray crystallography, but also demonstrate that ligand binding itself can induce the formation of a LBHB, as suggested by previous NMR studies in other systems [1,2,4]. We acknowledge that the crystalline environment can be different from solution. However, the fact that the LBHB is observed only in one of three structures obtained under the same crystallization conditions and is confirmed by computations in the present work suggests that a suitable microenvironment is necessary and sufficient for LBHB formation, and that the observed LBHB is not a crystallization artifact. Ultrahigh resolution X-ray crystal structures have been previously determined for other serine-based enzymes, such as the 0.78 Å apo subtilisin and 0.90 Å α-lytic protease bound by a covalent boronic acid inhibitor [39,40]. However, in these previous cases the proposed His-Asp LBHB appeared to be a short asymmetric HB based on both the HB lengths (2.62/2.73 Å) and the hydrogen positions [39,40], although in apo subtilisin, the histidine Nδ1-H bond of the HB donor appears slightly lengthened (1.2 Å). The catalytic serine is not involved in any LBHB in either of these two structures, similar to our apo and covalent complex structures.

It should be pointed out that more experimental evidence is needed to demonstrate the existence of a Lys73-Ser70 LBHB during the actual reaction pathway of Class A β-lactamase. If verified, the exact energetic contribution of this LBHB to catalysis still needs to be studied, computationally or experimentally. Whereas we interpreted the two complex structures in the context of the proposed reaction pathway, the structures might have instead captured states not relevant to the hydrolysis reaction. In particular, the LBHB we observed may be specifically induced by the non-covalent ligand used in our studies but not by the substrate. Previous QM/MM calculations also supported a competing acylation pathway using Glu166 and the catalytic water as the general base, with an energy barrier only 4 kcal/mol higher than the neutral Lys73 pathway discussed above [26]. However, the agreement between the structural details of our complexes and previous experimental and computational results seem to favor Lys73 as the general base in the substrate complex [19,23,24,26]. Whereas we believe the unique features of the compound are crucial in allowing us to trap such a stable LBHB in an otherwise usually transient state during catalysis, many of the key features, such as a partially negatively charged ring nitrogen, are also shared by the substrate and may hence be catalytically relevant.

LBHB in maintaining protein structure

The studies of LBHBs have so far only focused on their potential contribution to enzyme catalysis. In addition to the Ser70-Lys73 LBHB in the active site, we have also observed a LBHB in a near-surface yet buried region of the CTX-M protein between Asp233 and Asp246, present in all three structures. Again, we are able to observe the hydrogen shared by these two residues in the 2Fo−Fc density map, with a distance of 2.47 Å between the two heteroatoms (Fig. 4B). Asp233 and Asp 246 are highly conserved in Class A β-lactamases [41–43]. Based on the HB distance between these two residues, it appears that the LBHB may be present in many other Class A β-lactamases [16,44]. Because the two aspartate residues are located outside the active site, we suspect that the LBHB may be important for protein stability and may even play a role in protein folding. Interestingly, in a few enzymes where Asp246 is replaced by isoleucine, an alternative short hydrogen bond is formed

between Asp233 and Asp214 (Asn214 in CTX-M) [20,21]. It should be noted that hydrogen-mediated Asp-Asp pairs are commonly observed in proteins with some hypothesized to play a catalytic role as well [45]. These observations, together with previous studies on enzymes such as HIV protease and other Asp/Glu based enzymes, suggest that LBHB might play a common role in protein structure and function [45,46]. Ground-state and structural LBHBs, such as the one between Asp233 and Asp246, may offer valuable insights into the steric and energetic requirements for LBHB formation in proteins.

Discussion

The three ultrahigh resolution structures offer valuable insights into the protein microenvironment upon small molecule binding. These results have important implications for our understanding and modeling of protein-ligand interactions in enzyme catalysis, protein engineering and drug discovery. Non-covalent inhibitors are the focus of many structure-based ligand development approaches in the search for new drugs and chemical probes. In these computational modeling experiments, the effects of non-covalent ligand binding on residue protonation states are often ignored, particularly for side chains that do not form a direct HB with the ligand. None of the catalytic residues (i.e., Ser70, Lys73, and Glu166) establishes a HB with the non-covalent inhibitor, yet all undergo a protonation state change due to ligand binding. Additionally, there is no net proton gain/loss in the active site during the binding event, so the protonation state changes may not be captured by indirect methods such as ITC [47]. Both the experimental and computational data presented here suggest that virtual screening may potentially benefit from QM/MM methods in analyzing possible protonation state changes upon ligand binding [29].

The non-covalent CTX-M complex also answers the long-standing question of whether and how a LBHB can exist in a protein active site. The formation of a LBHB has several electrostatic and steric requirements. First, the two hydrogen bonding functional groups should have similar pKa's. In aqueous solution, the pKa of serine hydroxyl group is approximately 3 units higher than that of lysine amino group. However, in Class A β-lactamases, Ser70 resides at the N-terminus of a long stretch of α-helical structure (residues 69–87) and in close proximity to the oxyanion hole formed by the backbone amide groups of itself and Ser237 (Fig. 5A). In a few of our unpublished E166 mutant structures, Ser70's hydroxyl group is observed inside the oxyanion hole, suggesting transient HBs may be formed between Ser70 and the protein backbone in solution. Based on previous studies, this influence by the protein backbone, including both the dipole and the direct HBs, can significantly reduce the pKa of Ser70 side chain and bring it close to that of Lys73 [48]. A second important contributing factor to LBHB formation is desolvation of the active site upon binding **1**. LBHBs are not stable in bulk solvent because solvation effects from water would increase the charge separation between the two functional groups otherwise involved in LBHB, promoting proton transfer from one to the other [49]. These effects are likely to play a more important role in LBHBs where the two resonance structures (before vs after the proton transfer)have different electrostatic properties (e.g., (Lys73-NH_3)$^+$-(Ser70-O)$^-$ vs (Lys73-NH_2)-(Ser70-OH)), in comparison to those with two very similar or even identical resonance structures (e.g., (Asp233-COOH)-(Asp246-COO)$^-$ vs (Asp233-COO)$^-$-Asp246-COOH)). A recent study has demonstrated that changes in solvent dielectric (e.g., water vs

chloroform) do not significantly affect HB lengths in small-molecule model systems[50], suggesting that desolvation of a protein binding pocket cannot alone account for LBHB formation. As the authors note however, many protein binding sites (and catalytic sites in particular) are far from a homogeneous low-dielectric environment. Rather, catalytic sites in particular possess a highly orchestrated arrangement of hydrogen bonds and dipolar or charged groups that, together with desolvation, serve to alter the pKa values of side chain residues and in specific cases reduce ΔpKa values such that LBHB formation is enabled. In our protein, despite the observation of two structural waters including the catalytic water bound by the catalytic residues, the binding of the non-covalent inhibitor **1** completely isolates the CTX-M active site from bulk solvent (Fig. 5A). This effect is illustrated by the loss of the HB between the catalytic water (wat1) and the water molecule (wat2) closer to bulk solvent in the apo structure (Fig. 3A). Additionally, the binding of both the non-covalent and covalent inhibitors causes a slight contraction of the active site, as shown by the small movement of the catalytic water (1.2 Å) and of Glu166 and Asn170 (0.5–0.6 Å) (Fig. 3D). This slightly higher compactness of the active site squeezes out the water (wat3) shared by Lys73 and Glu166 in the apo structure (Fig. 3A). Lastly, despite the compactness of the active site, small movements of Ser70 and Lys73 side chains in concert with adjustments in other polar interactions appear to be sufficient to allow these residues to adopt the optimal geometry necessary for LBHB formation.

For serine-based enzymes, Cleland and Kreevoy previously hypothesized that a direct LBHB between the general base and the nucleophilic serine can stabilize the activated serine during its attack on the substrate, while conceding that this LBHB might be difficult to capture by experiment due to its transient nature [1]. Our non-covalent complex offers the first, albeit slightly complicated, example of such a LBHB due to the concerted base mechanism involving both Glu166 and Lys73. During the acylation process and immediately following ligand binding, Glu166 is responsible for the initial deprotonation of Ser70 while Ser70 concurrently takes a proton from Lys73. However, if we only consider the pre-covalent intermediate with neutral (Lys73-NH_2)-(Ser70-OH) as predicted by previous QM/MM calculations [26], Lys73 is the de facto general base and clearly plays a more important role in this process. In fact, neutral Lys73 has been shown by biochemical analysis and NMR to function as a general base for acylation in E166A mutants of Class A β-lactamases like TEM-1, as well as in penicillin-binding proteins (PBPs), the bacterial target of β-lactam antibiotics. [23,51] Serine β-lactamases have evolved from PBPs and the two groups of enzymes often share the same catalytic residues [52]. One of the only, and significant, exceptions is Glu166, which is unique for Class A β-lactamases and essential for their ability to catalyze the deacylation step of β-lactam hydrolysis. The E166A mutant β-lactamases are defective in the deacylation reaction, similar to the PBPs. As previously discussed by others, Glu166's role in the complicated acylation mechanism may have been an evolutionary relic instead of a catalytic necessity [26]. Because Glu166 is neutral in the non-covalent complex, its influence on neighboring residues' pKa is reduced compared with a charged Glu166 in the apo state. It is likely that the electrostatic microenvironment of the pre-covalent Michaelis complex is similar between Class A β-lactamases and PBPs. We therefore hypothesize that a LBHB between the equivalents of Ser70 and Lys73 may also play an important role in the catalysis of at least some PBPs, including their inhibition by β-

lactam antibiotics. Moreover, as nucleophilic serine is used to catalyze a wide range of enzymatic reactions by forming a covalent intermediate with the substrate, it is possible that similar LBHBs are present in other enzymatic reactions, as previously hypothesized [1,4,53].

It is worth noting that even the strongest critics of the LBHB hypothesis acknowledge that LBHB may be involved in catalysis by specific enzymes. Their key criticism centers on whether LBHBs or other preorganized active site features are the main stabilizing factor of enzyme catalysis[49,54]. Our structures suggest that the reaction catalyzed by Class A β-lactamases may utilize both a LBHB (between Ser70 and the general base in the substrate complex, Lys73) and preorganized polar groups, such as the oxyanion hole formed by the backbone atoms of Ser70 and Ser237. Importantly, the non-covalent complex structure offers insights into the polarity of the enzyme active site that has been much debated in previous discussions[55]. Together with two QM/MM calculations, the experimental structure demonstrates that the desolvated enzyme active site is only weakly polar and favors less net-charge separation in side chain functional groups, resulting in the protonation state changes in Glu166, Lys73 and Ser70. A LBHB not only can exist in this environment in the presence of the right substrate/ligand, but also may contribute to a lower-energy TS by further reducing the negative charge accumulation on the tetrahedral intermediate. In the absence of the LBHB between Ser70 and the general base Lys73, the tetrahedral TS oxyanion has a net charge of −1. With the LBHB, Ser70 is only partially deprotonated and the TS oxyanion has a net charge of approximately −1/2 if it occurs in the midst of the proton transfer. We therefore suggest that LBHB involving proton transfer in progress can indeed be a unique feature of enzyme catalysis by altering the TS in the weakly polar protein microenvironment, in comparison to reaction pathways where the proton transfer is completed prior to the TS. We postulate that this mechanism may be broadly employed by enzymes in general acid/base catalysis with conducive electrostatic/steric microenvironments in the active site, similar to previous hypotheses [53,56]. However, the exact energetic contribution of this LBHB to enzymatic general catalysis remains to be studied in detail, particularly in comparison to other short HBs. Previous studies have demonstrated a continuum of short hydrogen bonds from short ionic HBs where the hydrogen is clearly covalently bonded to one heteroatom, HBs with partially delocalized hydrogens (lengthened bond length between the hydrogen and the heteroatom), symmetrical LBHBs with two potential energy minima separated by a shallow barrier along the HB, to single-well HBs [56,57]. It is likely that there is a continuum of energy contribution from these different HBs to catalysis including general catalysis, depending on the specific reaction mechanism.

In summary, the three sub-Angstrom resolution structures of CTX-M presented here have captured protonation state changes and LBHB formation induced by non-covalent ligand binding. Although these studies cannot resolve all of the controversy surrounding the role of LBHBs in enzyme catalysis, they do suggest that LBHBs can be induced by a conducive protein microenvironment in particular enzymes. More specifically, the results support a 20-year old hypothesis by Cleland and Kreevoy that a transient and direct LBHB can be used to stabilize an activated nucleophilic serine in its attack on a substrate [1]. The protonation state change induced by both non-covalent and covalent inhibitors has important implications for

how we simulate protein-ligand interactions in molecular docking and may lead to better performance of structure-based approaches in drug discovery and enzyme engineering.

Methods

Protein purification, crystallization and structure determination

To improve crystal qualities and diffraction resolutions and to ensure full ligand occupancies, we tested in our experiments multiple proteins and purification protocols (CTX-M-9, His-tag CTX-M-9, codon-optimized CTX-M-9 without signal peptide, CTX-M-14), different crystallization conditions and crystal forms (space group $P2_12_12_1$ at pH 3.0–5.5, $P2_1$ and $P3_221$ at pH 7.9–8.7), various procedures to prepare complex crystals (co-crystallization, and soaking at different compound concentrations and for varying lengths of time), four non-covalent and four covalent inhibitors, and multiple beamlines and data collection strategies. Approximately 200 crystals were screened for X-ray diffraction and 20 Sub-Angstrom resolution data sets were analyzed.

In the final optimized protocol, CTX-M-14 was used to represent the CTX-M family. The protein was purified as previously described [58] and crystallized in 1.0–1.2M potassium phosphate buffer (pH 8.3) from hanging drops at 20°C. At pH 8.3, CTX-M-14 retains half of its activity (k_{cat}/K_m) compared with pH 7.0, suggesting that the protonation states of active site residues should not differ significantly between the two pHs. This is consistent with the fact that β-lactamases need to function over a range of pHs in the fluctuating environments of bacterial periplasm. The final concentration of the protein in the drop ranged from 6.5 mg ml^{-1} to 10 mg ml^{-1}. The non-covalent complex crystals were obtained through soaking methods, with compound concentrations of 5.0mM and soaking times ranging from approximately 24 to 48 hours. The complex crystals with the boronic acid inhibitor (compound **2**) were obtained with co-crystallization with the protein, with the final concentration of the compound in the drop at 5.0mM. Diffraction was measured at two beamlines: 8.3.1 at Advanced Light Source (ALS), Berkeley, California and 23-ID-B of GM/CA@APS at Advanced Photon Source (APS), Argonne, Illinois. Data were indexed, scaled and merged with HKL2000 [59]. The apo and complex structures were refined with SHELX97 [60]. Model rebuilding was performed using Coot [61]. Electron density maps were generated using SHELXPRO with the sharpening option. The figures were generated using PyMOL [62]. Ligand occupancy was refined for all complex structures and was observed to be at or near 100% (98%–103%) for all the ligands in the active site. For the non-covalent complex, a second copy of the ligand was observed stacking on top of the one inside the active site, a crystallization artifact due to the high compound concentrations used to ensure full ligand occupancy. This artifact, however, does not affect the active site hydrogen bonding network when compared to the same complex prepared using lower inhibitor concentrations, based on the bond and HB lengths of active site residues in the presence and absence of the second copy of the inhibitor. The second copy of the inhibitor also resides outside the active site and does not form any interactions with the active site residues.

Computational methods and pathway determination

The cocrystallized non-covalent structure of the tetrazole-based inhibitor and CTX-M β-lactamase (PDB:4UA7) was initially processed using www.charmming.org [63]. CHARMM [31] c36a6 was used to prepare the protein, add hydrogens, and assign ionizable protonation states [64,65]. Parameters for the non-covalent inhibitor were obtained from paramchem.org, which were reordered to satisfy the requirements of the Domain Decomposition (DOMDEC) [66] molecular dynamics (MD) parallelization module in CHARMM. Three protonation state combinations were created using the PATCh command to best capture active site behavior: state **I** --- Ser70: negatively charged side chain (deprotonated), Glu166: neutral, and Lys73: positively charged side chain (protonated); state **II** --- Ser70: neutral, Glu166: neutral, Lys73: neutral; and state **III** --- Ser70: neutral, Glu166: negatively charged side chain (deprotonated), and Lys73: positively charged side chain (protonated). Additionally, an apo state was prepared mimicking protonation state **III**. The CHARMM22 [67] and CHARMM36 [68] generalized force fields (C22 and CGenFF) were used in combination with the FLEXible parameter reader. The protein, crystallized waters, and non-covalent inhibitor were appended together, which was followed by an initial steepest descent minimization (200 steps) where all heavy atoms in the protein and ligand were fixed. The structures were solvated in a cubic water box using TIP3P waters. Again this was followed by a partial steepest descent minimization of 50 steps allowing the system to relax. Solvation was followed by an iterative Monte Carlo neutralization of the system where water molecules were replaced by potassium and chloride ions at random to yield a charge neutral system with a final salt concentration of 0.15 M. Following each iteration a short minimization (25 steps) was performed and compared to previous steps. After four iterations, the lowest energy structure was retained and minimized using the adopted basis Newton-Raphson (ABNR) method to a gradient tolerance of 0.001 kcal/mol•Å where all bonds involving hydrogen were fixed. The minimized structure was heated from 110.15 K to 310.15 K (body temperature) over 100 ps. Finally the system was equilibrated for 11 ns using DOMDEC at constant pressure (1 atm) and temperature (310.15 K).

Following the MD simulations, extensive RMSD and distance analysis were performed. A representative structure (based on side chain distances) was chosen and minimized using a hybrid quantum mechanics/molecular mechanics (QM/MM) potential until a 0.005 kcal/mol•Å rms gradient tolerance was achieved. During the minimization the non-covalent inhibitor, Glu166, Ser70, Lys73, Lys234, Thr235, Gly236, Ser237, H_2O26, and H_2O45 were included in the QM region. Link atoms were placed between residues and two atoms in the residue specified in the following notation: residue number QM atom/MM atom (standard topology notation). Here are the link atom cuts for the QM region in the present work: 233 C/CA, 238 CA/C, 69 C/CA, 74 CA/CB, 74 CA/C, 166 CA/C, 170 CA/C, 165 C/CA, and 169 C/CA. The QM region (over 200 atoms) was treated with the ωB97X-D functional [69] and a 6-31G* basis set. QM/MM minimizations were carried out with the Q-Chem/CHARMM QM/MM interface [31–33].

The characterization of the low barrier hydrogen bond between Ser70 and Lys73 was further elucidated by computing the energy barrier of the proton transfer between these two residues. During state **I**'s QM/MM minimization charged Lys73 becomes neutral as the

hydrogen spontaneously transfers to the Ser70 to stabilize the excess negative charge. It is state **I**'s QM/MM minimized structure that most closely resembles the experimental crystal structure active site; therefore, it is the starting structure for the RPATH [34]+RESD computations[30] used to compute the barrier. The QM region used for the reaction path calculations is the same as the QM/MM minimizations with the replicated region defined to be 6.5 Å around the QM region. The reaction pathway was constructed by defining two replicas. Replica 1 is defined as the reactant: neutral Ser70 and Lys73 (i.e., no restraints on hydrogen position). The hydrogen is then restrained to move along the reaction path using a linear combination of distances: $\delta = d_{\text{Ser70 O - Ser70 H}} - d_{\text{Ser70 H - Lys73 N}}$ to the product state: charged Ser70 and Lys73. Replica 2 is defined as a point along the reaction pathway as δ is increased by 0.1 Å; this process is repeated until the proton transfer is complete. Replica 1 and replica 2 were minimized with δ ranging from −0.52 Å – 0.28 Å. QM/MM single point energies were recomputed for the entire pathway using the ωB97X-D/6-311++G** level [69,70] of theory. A previously established method[35] used to determine highly accurate low barrier hydrogen bond energy barriers was replicated in the present work. The test set in that work included malonaldehyde and seven of its derivatives, herein these were recomputed at the ωB97X-D/6-311++G** level of theory to obtain a new linear regression ($\Delta Eb_{\text{corr}} = 1.10\Delta Eb_{\omega\text{B97X-D}} + 0.09$) that was used to predict the proton transfer barrier with improved (i.e., approximate focal point) accuracy.

Supplementary Material

Refer to Web version on PubMed Central for supplementary material.

Acknowledgments

We thank Shahriar Mobashery, Jed Fisher, and Wayne Guida for insightful discussions, and Orville Pemberton for reading the manuscript. This work has been supported by the NIH (AI103158 to Y.C.). GM/CA@APS has been funded in whole or in part with Federal funds from the National Cancer Institute (ACB-12002) and the National Institute of General Medical Sciences (AGM-12006). Use of the Advanced Photon Source was supported by the U.S. Department of Energy, Basic Energy Sciences, Office of Science, under contract No. W-31-109-ENG-38. HLW3 would like to acknowledge the generous support of NIH (1K22HL088341-01A1), NSF CHE (1156853), and the University of South Florida (start-up). Computations were performed at the USF Research Computing Center and using XSEDE computational resources (MCB120133); both centers are greatly appreciated.

References

1. Cleland WW, Kreevoy MM. Science. 1994; 264:1887. [PubMed: 8009219]
2. Halkides CJ, Wu YQ, Murray CJ. Biochemistry. 1996; 35:15941. [PubMed: 8961961]
3. Graham JD, Buytendyk AM, Wang D, Bowen KH, Collins KD. Biochemistry. 2014; 53:344. [PubMed: 24359447]
4. Frey PA, Whitt SA, Tobin JB. Science. 1994; 264:1927. [PubMed: 7661899]
5. Westler WM, Weinhold F, Markley JL. J Am Chem Soc. 2002; 124:14373. [PubMed: 12452711]
6. Ogata Y, Daido M, Kawashima Y, Tachikawa M. Rsc Advances. 2013; 3:25252.
7. Nadal-Ferret M, Gelabert R, Moreno M, Lluch JM. J Am Chem Soc. 2014; 136:3542. [PubMed: 24548066]
8. Chaudret R, Cisneros GA, Parisel O, Piquemal JP. Chemistry. 2011; 17:2833. [PubMed: 21308813]
9. Feldblum ES, Arkin IT. Proc Natl Acad Sci U S A. 2014; 111:4085. [PubMed: 24591597]
10. Ash EL, Sudmeier JL, De Fabo EC, Bachovchin WW. Science. 1997; 278:1128. [PubMed: 9353195]

11. Guthrie JP. Chem Biol. 1996; 3:163. [PubMed: 8807842]
12. Ishida T. Biochemistry. 2006; 45:5413. [PubMed: 16634622]
13. Schutz CN, Warshel A. Proteins. 2004; 55:711. [PubMed: 15103633]
14. Natarajan A, Schwans JP, Herschlag D. J Am Chem Soc. 2014; 136:7643. [PubMed: 24787954]
15. Nichols DA, Jaishankar P, Larson W, Smith E, Liu G, Beyrouthy R, Bonnet R, Renslo AR, Chen Y. J Med Chem. 2012; 55:2163. [PubMed: 22296601]
16. Chen Y, Bonnet R, Shoichet BK. J Am Chem Soc. 2007; 129:5378. [PubMed: 17408273]
17. Bonnet R. Antimicrob Agents Chemother. 2004; 48:1. [PubMed: 14693512]
18. Chen Y, Shoichet B, Bonnet R. J Am Chem Soc. 2005; 127:5423. [PubMed: 15826180]
19. Strynadka NC, Adachi H, Jensen SE, Johns K, Sielecki A, Betzel C, Sutoh K, James MN. Nature. 1992; 359:700. [PubMed: 1436034]
20. Minasov G, Wang X, Shoichet BK. J Am Chem Soc. 2002; 124:5333. [PubMed: 11996574]
21. Nukaga M, Mayama K, Hujer AM, Bonomo RA, Knox JR. J Mol Biol. 2003; 328:289. [PubMed: 12684014]
22. Escobar WA, Tan AK, Lewis ER, Fink AL. Biochemistry. 1994; 33:7619. [PubMed: 7912106]
23. Golemi-Kotra D, Meroueh SO, Kim C, Vakulenko SB, Bulychev A, Stemmler AJ, Stemmler TL, Mobashery S. J Biol Chem. 2004; 279:34665. [PubMed: 15152012]
24. Lietz EJ, Truher H, Kahn D, Hokenson MJ, Fink AL. Biochemistry. 2000; 39:4971. [PubMed: 10819961]
25. Guillaume G, Vanhove M, Lamotte-Brasseur J, Ledent P, Jamin M, Joris B, Frere JM. J Biol Chem. 1997; 272:5438. [PubMed: 9038144]
26. Meroueh SO, Fisher JF, Schlegel HB, Mobashery S. J Am Chem Soc. 2005; 127:15397. [PubMed: 16262403]
27. Howard EI, Sanishvili R, Cachau RE, Mitschler A, Chevrier B, Barth P, Lamour V, Van Zandt M, Sibley E, Bon C, Moras D, Schneider TR, Joachimiak A, Podjarny A. Proteins. 2004; 55:792. [PubMed: 15146478]
28. Tomanicek SJ, Standaert RF, Weiss KL, Ostermann A, Schrader TE, Ng JD, Coates L. J Biol Chem. 2013; 288:4715. [PubMed: 23255594]
29. Hargis JC, White JK, Chen Y, Woodcock HL. J Chem Inf Model. 2014; 54:1412. [PubMed: 24697903]
30. Woodcock HL, Hodoscek M, Brooks BR. J Phys Chem A. 2007; 111:5720. [PubMed: 17555303]
31. Brooks BR, Brooks CL III, MacKerell AD Jr, Nilsson L, Petrella RJ, Roux B, Won Y, Archontis G, Bartels C, Boresch S, Caflisch A, Caves L, Cui Q, Dinner AR, Feign M, Fischer S, Gao J, Hodošček M, Im W, Kuczera K, Lazaridis T, Ma J, Ovchinnikov V, Paci E, Pastor RW, Post CB, Pu JZ, Schaefer M, Tidor B, Woodcock HL III, Wu X, Yang W, York DM, Karplus M. J Comp Chem. 2009; 30:1545. [PubMed: 19444816]
32. Shao Y, Fusti-Molnar L, Jung Y, Kussmann J, Ochsenfeld C, Brown ST, Gilbert ATB, Slipchenko LV, Levchenko SV, O'Neill DP, Distasio RA, Lochan RC, Wang T, Beran GJO, Besley NA, Herbert JM, Lin CY, Van Voorhis T, Chien SH, Sodt A, Steele RP, Rassolov VA, Maslen PE, Korambath PP, Adamson RD, Austin B, Baker J, Byrd EFC, Daschel H, Doerksen RJ, Dreuw A, Dunietz BD, Dutoi AD, Furlani TR, Gwaltney SR, Heyden A, Hirata S, Hsu C-P, Kedziora G, Khalliulin RZ, Klunzinger P, Lee AM, Lee MS, Liang W, Lotan I, Nair N, Peters B, Proynov EI, Pieniazek PA, Rhee YM, Ritchie J, Rosta E, Sherrill DC, Simmonett AC, Subotnik JE, Woodcock HL III, Zhang W, Bell AT, Chakraborty AK, Chipman DM, Keil FJ, Warshel A, Hehre WJ, Schaefer HF III, Kong J, Krylov AI, Gill PMW, Head-Gordon M. Phys Chem Chem Phys. 2006; 8:3172. [PubMed: 16902710]
33. Woodcock HL III, Hodošček M, Gilbert ATB, Gill PMW, Schaefer HF III, Brooks BR. J Comp Chem. 2007; 28:1485. [PubMed: 17334987]
34. Woodcock HL, Hodošček M, Sherwood P, Lee YS, Schaefer HF III, Brooks BR. Theor Chem ACC. 2003; 109:140.
35. Hargis JC, Evangelista FA, Ingels JB, Schaefer HF. J Am Chem Soc. 2008; 130:17471. [PubMed: 19049282]

36. Adediran SA, Deraniyagala SA, Xu Y, Pratt RF. Biochemistry. 1996; 35:3604. [PubMed: 8639512]
37. Yamaguchi S, Kamikubo H, Kurihara K, Kuroki R, Niimura N, Shimizu N, Yamazaki Y, Kataoka M. Proc Natl Acad Sci U S A. 2009; 106:440. [PubMed: 19122140]
38. Saito K, Ishikita H. Proc Natl Acad Sci U S A. 2012; 109:167. [PubMed: 22173632]
39. Kuhn P, Knapp M, Soltis SM, Ganshaw G, Thoene M, Bott R. Biochemistry. 1998; 37:13446. [PubMed: 9753430]
40. Fuhrmann CN, Daugherty MD, Agard DA. J Am Chem Soc. 2006; 128:9086. [PubMed: 16834383]
41. Verma D, Jacobs DJ, Livesay DR. PLoS Comput Biol. 2013; 9:e1003155. [PubMed: 23874193]
42. Toth M, Smith C, Frase H, Mobashery S, Vakulenko S. J Am Chem Soc. 2010; 132:816. [PubMed: 20000704]
43. Risso VA, Gavira JA, Mejia-Carmona DF, Gaucher EA, Sanchez-Ruiz JM. J Am Chem Soc. 2013; 135:2899. [PubMed: 23394108]
44. Ke W, Bethel CR, Thomson JM, Bonomo RA, van den Akker F. Biochemistry. 2007; 46:5732. [PubMed: 17441734]
45. Das A, Prashar V, Mahale S, Serre L, Ferrer JL, Hosur MV. Proc Natl Acad Sci U S A. 2006; 103:18464. [PubMed: 17116869]
46. Langkilde A, Kristensen SM, Lo Leggio L, Molgaard A, Jensen JH, Houk AR, Navarro Poulsen JC, Kauppinen S, Larsen S. Acta Crystallogr, Sect D: Biol Crystallogr. 2008; D64:851. [PubMed: 18645234]
47. Czodrowski P, Sotriffer CA, Klebe G. J Mol Biol. 2007; 367:1347. [PubMed: 17316681]
48. Lockhart DJ, Kim PS. Science. 1993; 260:198. [PubMed: 8469972]
49. Warshel A, Papazyan A. Proc Natl Acad Sci U S A. 1996; 93:13665. [PubMed: 8942991]
50. Sigala PA, Ruben EA, Liu CW, Piccoli PM, Hohenstein EG, Martinez TJ, Schultz AJ, Herschlag D. J Am Chem Soc. 2015; 137:5730. [PubMed: 25871450]
51. Zhang W, Shi Q, Meroueh SO, Vakulenko SB, Mobashery S. Biochemistry. 2007; 46:10113. [PubMed: 17685588]
52. Meroueh SO, Minasov G, Lee W, Shoichet BK, Mobashery S. J Am Chem Soc. 2003; 125:9612. [PubMed: 12904027]
53. Cleland WW. Arch Biochem Biophys. 2000; 382:1. [PubMed: 11051090]
54. Warshel A. J Biol Chem. 1998; 273:27035. [PubMed: 9765214]
55. Warshel A, Papazyan A, Kollman PA. Science. 1995; 269:102. [PubMed: 7661987]
56. Schowen KB, Limbach HH, Denisov GS, Schowen RL. Biochim Biophys Acta. 2000; 1458:43. [PubMed: 10812024]
57. Perrin CL, Nielson JB. Annu Rev Phys Chem. 1997; 48:511. [PubMed: 9348662]
58. Chen Y, Delmas J, Sirot J, Shoichet B, Bonnet R. J Mol Biol. 2005; 348:349. [PubMed: 15811373]
59. Otwinowski Z, Minor W. Methods Enzymol. 1997; 276:307.
60. Sheldrick GM, Schneider TR. Methods Enzymol. 1997; 277:319. [PubMed: 18488315]
61. Emsley P, Cowtan K. Acta Crystallogr, Sect D: Biol Crystallogr. 2004; 60:2126. [PubMed: 15572765]
62. The PyMOL Molecular Graphics System, Version 1.5.0.4. Schrödinger, LLC;
63. Miller BT, Singh RP, Klauda JB, Hodošček M, Brooks BR, Woodcock HL III. J Chem Inf Model. 2008; 48:1920. [PubMed: 18698840]
64. Vanommeslaeghe K, MacKerell AD Jr. J Chem Inf Model. 2012; 52:3144. [PubMed: 23146088]
65. Vanommeslaeghe K, Raman EP, MacKerell AD Jr. J Chem Inf Model. 2012; 52:3155. [PubMed: 23145473]
66. Hynninen AP, Crowley MF. J Comp Chem. 2013; 35:413.
67. MacKerell AD Jr, Bashford D, Bellott M, Dunbrack RL Jr, Evanseck JD, Field MJ, Fischer S, Gao J, Guo H, Ha S, Joseph-McCarthy D, Kuchnir L, Kuczera K, Lau FTK, Mattos C, Michnick S, Ngo T, Nguyen DT, Prodhom B, Reiher WE III, Roux B, Schlenkrich M, Smith JC, Stote R,

Straub J, Watanabe M, Wiorkiewicz-Kuczera J, Yin D, Kraplus M. J Phys Chem. 1998; B102:3586.

68. Vanommeslaeghe K, Hatcher E, Acharya C, Kundu S, Zhong S, Shim J, Darian E, Guvench O, Lopes P, Vorobyov I, MacKerell AD Jr. J Comp Chem. 2010; 31:671. [PubMed: 19575467]
69. Chai JD, Head-Gordon M. Phys Chem Chem Phys : PCCP. 2008; 10:6615. [PubMed: 18989472]
70. Harihara PC, Pople JA. Theor Chim Acta. 1973; 28:213.

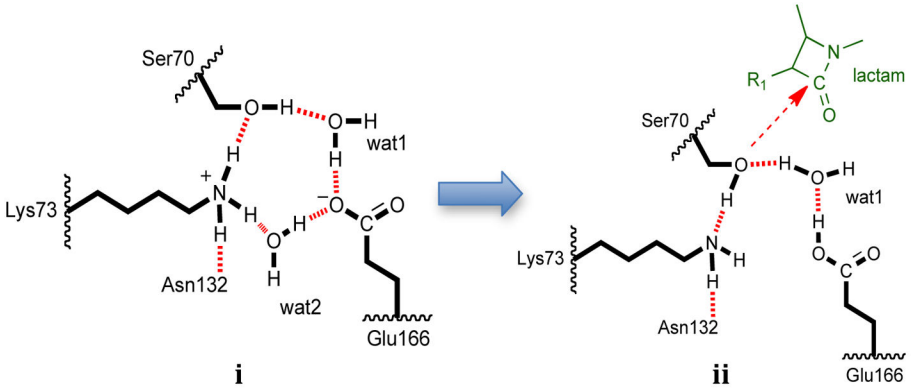

Figure 1. A concerted base hypothesis for the acylation half–reaction of Class A β--lactamase proposes protonation state changes prior to general acid/base catalysis

Beginning with the apo enzyme hydrogen bonding network (i) to a ground-state Michaelis complex (ii), as predicted by QM/MM calculations. The binding of the substrate is proposed to change the protonation states of Ser70, Lys73 and Glu166. A neutral Lys73 then serves as the general base to activate Ser70. The remaining stages of catalysis (stages not shown) proceed through a high-energy acylation transition state, to a low-energy acyl-enzyme intermediate. Subsequently, deacylation proceeds through a high-energy transition state and on to a post-covalent product complex.

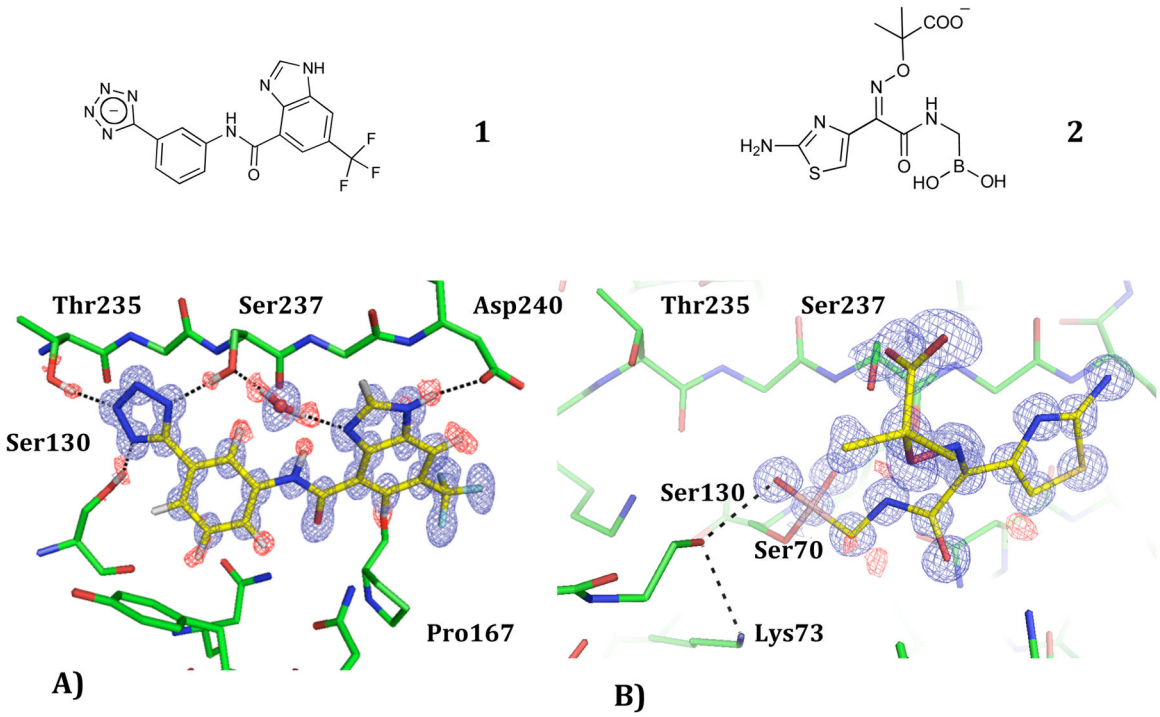

Figure 2. Complex structures of CTX-M β-lactamase

The 2Fo−Fc (blue) and Fo−Fc (red) electron density maps of the ligands are contoured at 1.5 and 2 σ respectively. The positive difference peaks indicate the positions of hydrogen atoms. (A) The non-covalent complex with tetrazole-based inhibitor **1**. The catalytic machinery, including Ser70 and Lys73, is directly behind the ligand and isolated from the bulk solvent. (B) The complex structure of boronic acid inhibitor **2**, mimicking the acylation transition state tetrahedral intermediate.

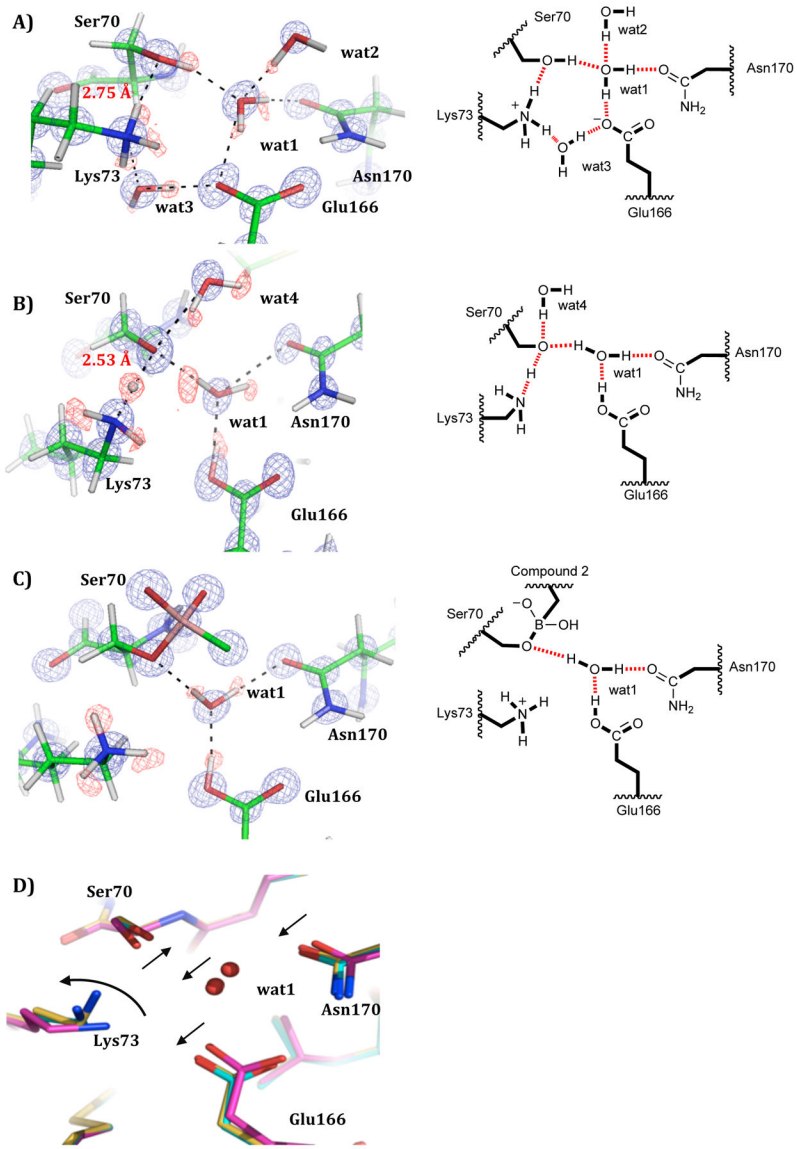

Figure 3. Proton transfer and short hydrogen bond formation induced by ligand binding

Only the catalytic residues are shown. Wat1 is the catalytic water. The 2Fo−Fc maps (blue) are contoured at 1.5 σ. The positive Fo−Fc peaks (red, 2 σ) indicate the positions of hydrogen atoms. (A) Apo structure at 0.79 Å. (B) Structure of non-covalent complex with compound **1** at 0.89 Å. The hydrogen between Ser70 and Lys73 is located at equal distances from the two electronegative atoms. (C) Structure of covalent complex with compound **2** at 0.84 Å. (D) Three structures superimposed, showing the movement of Lys73 (apo, magenta; non-covalent complex, yellow; covalent complex, cyan). The arrows indicate residue movements from the apo structure to the two complexes.

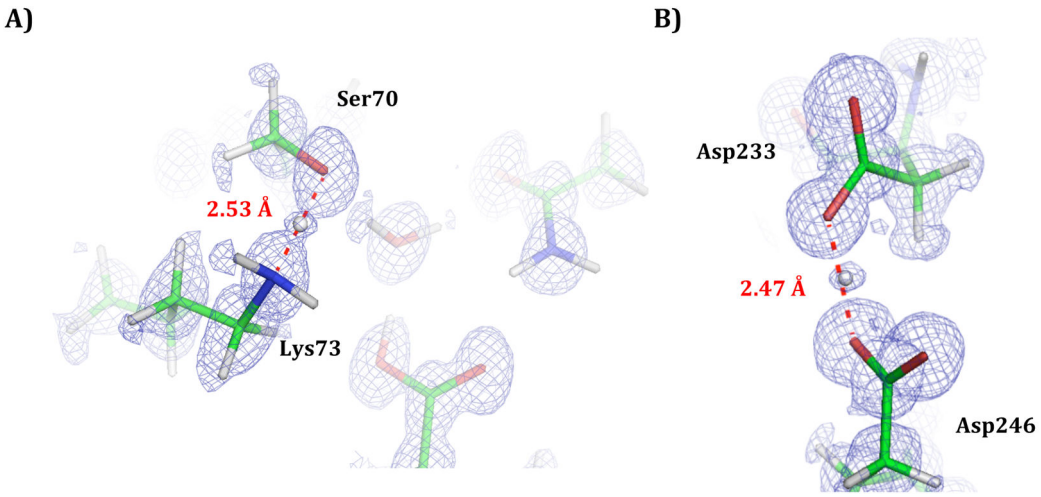

Figure 4. Hydrogen atoms captured in 2Fo−Fc electron density maps

The small isolated peaks indicate well-ordered hydrogen atoms on carbon atoms and two hydrogens involved in LBHB. The maps are contoured at 0.5 σ to show the center of those peaks for LBHB hydrogens and to eliminate background noise. More protons can be identified in Fo−Fc maps (not shown here). (A) LBHB between Lys73 and the catalytic Ser70 in the active site. The angles involving the HB are ∠ Ser70Cβ-Ser70Oγ-H (111.7°), ∠ Ser70Oγ-H-Lys73Nζ (175.4°), and ∠ H-Lys73Nζ-Lys73Cε (114.5°). (B) LBHB involving Asp233 and Asp246. Both residues are buried with Asp233 near the protein surface but shielded from bulk solvent by Arg222 in the crystal structures. Asp246 is located deeper and closer to the protein core, and is replaced by an isoleucine in some Class A β-lactamases. The angles involving the HB are ∠ Asp233Cγ-Asp233Oδ1-H (113.9°), ∠ Asp233Oδ1-H-Asp246Oδ2 (167.0°), and ∠ H-Asp246Oδ2-Asp246Cγ (116.9°)

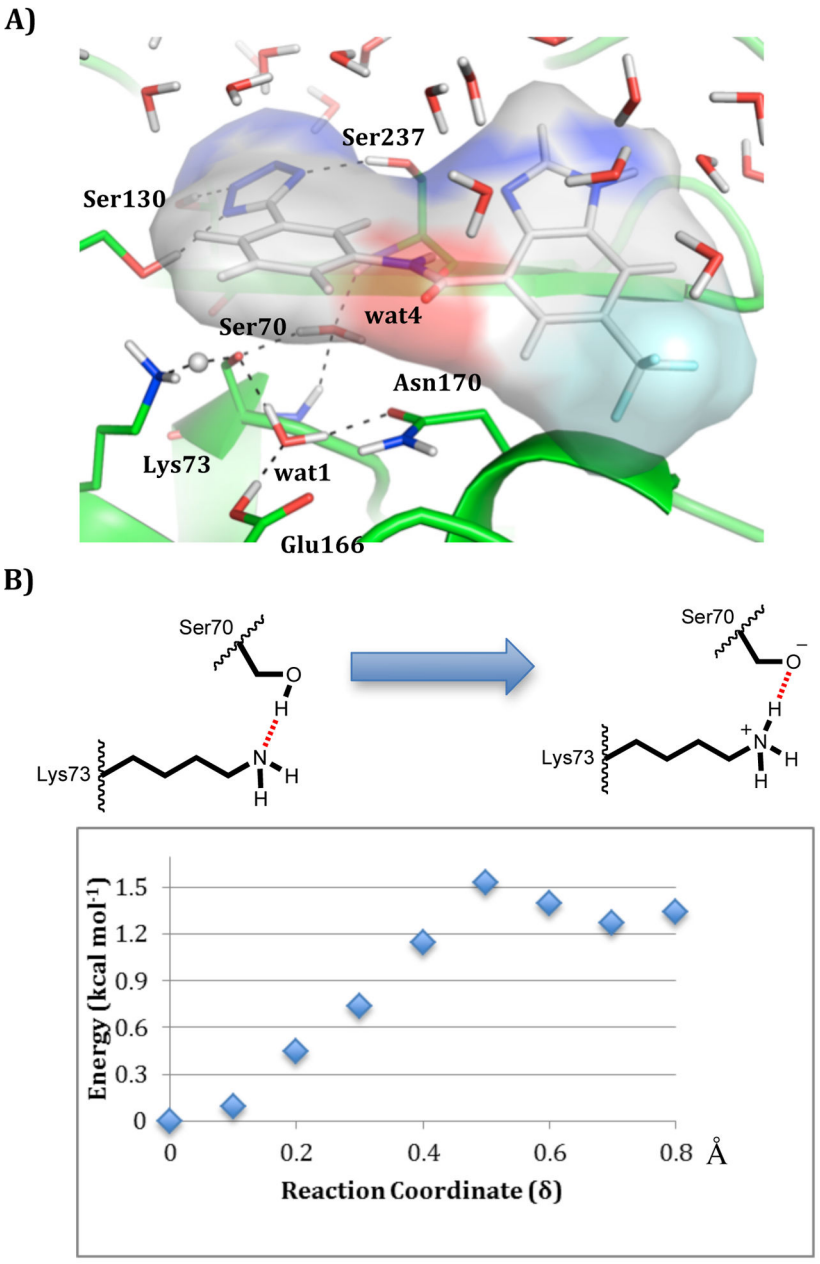

Figure 5. QM/MM Transition State and Reaction Pathway

QM/MM Replica path + Restraint Distance calculations determined the proton transfer barrier occurring between Ser70 and Lys73. A) The transition state of the proton transfer with the proton located in the middle between the two electronegative atoms. Wat1 is the catalytic water and wat4 is located in the oxyanion hole formed by the backbone amide groups of Ser70 and Ser237. Ser70 is positioned at the N-terminus of a helix. B) The reaction path plotted as a function of the QM/MM energy for the proton transfer barrier. The hydrogen is moved from Ser70 (0.0 Å) to Lys73 (0.8 Å).